Networks and Heterogeneous Media

NHM, 19(2): 753–770.
DOI: 10.3934/nhm.2024034
Received: 25 May 2024
Revised: 11 July 2024
Accepted: 18 July 2024
Published: 25 July 2024

https://www.aimspress.com/journal/nhm

Research article

Natural convection flow and heat transfer of generalized Maxwell fluid with distributed order time fractional derivatives embedded in the porous medium

Jinhu Zhao*

School of Mathematics and Statistics, Fuyang Normal University, Fuyang 236037, Anhui, China

* **Correspondence:** Email: jinhuzhao@fynu.edu.cn.

Abstract: Numerical simulation was performed for unsteady natural convection flow and heat transfer in a porous medium using the generalized Maxwell model and fractional Darcy's law with distributed order time fractional derivatives. The finite volume method combined with the fractional *L1* scheme was used to solve strongly coupled governing equations with nonlinear fractional convection terms. Numerical solutions were validated via grid independence tests and comparisons with special exact solutions. The effects of porosity, Darcy number, and relaxation time parameters on transport fields are presented. The results illustrate that porosity and permeability have opposite influences on temperature and velocity profiles. Moreover, the relaxation time parameters have remarkable effects on velocity profiles, and the variations possess significant differences.

Keywords: generalized Maxwell fluid; distributed order time fractional derivatives; porous medium; finite volume method

1. Introduction

Transport phenomena in porous media have widespread applications throughout manifold aspects of nature and industrial engineering, such as groundwater utilization, oil and gas extraction, chemical industry, building materials, biomedical development, etc. [1–2]. The relevant studies on heat transfer theory also permeate many scientific and technical fields [3]. On account of the structural complexity

inside porous media and the diversity of fluids, convective flow and heat transfer in porous media have strongly nonlinear characteristics, and the classical linear Darcy's law is not applicable. Moreover, the coupled effects of velocity and temperature fields have important influences on the heat transfer process. Because of this, a novel constitutive equation and heat transfer model should be derived to characterize and simulate the internal physical mechanism inside the porous medium.

For the last few years, constitutive relationship equations with fractional derivatives have been frequently adopted in the description of complex dynamics [4–7], and simultaneously relevant research on fractional porous media has also been carried out widely. Wei et al. [8] proposed two fractional derivative models to describe non-Darcy flow in porous media. Yang et al. [9] discussed anomalous imbibition of non-Newtonian fluid in a porous medium by a spatiotemporal fractional model. Ahmed [10] used Caputo fractional derivatives to govern the mixed convective flow of hybrid nanofluids together with the Darcy model. Ai et al. [11] presented a viscoelastic model with fractional derivatives to simulate multilayered cross-anisotropic porous media. Jiang et al. [12] solved the governing equations of fractional second-grade fluid through a porous medium. Jiang et al. [13] developed a fractional Burgers model to simulate non-Newtonian fluid in porous media with complex physical-chemical conditions.

Nevertheless, the restrictions of the mentioned research are fixed fractional derivative parameters that manifest a rather limited class of memory characteristics and nonlocal properties [14]. Recent developments in various fields, such as thermal management, manufacturing, blood flow, etc., emphasize the need to resolve the limitations of conventional models. The convective flow and heat transfer problems of viscoelastic fluids involve complex molecule internal structures and multi-scale effects. Therefore, the distributed order fractional derivative that was proposed by Caputo to develop the fractional derivative models [15] has been frequently applied to boundary layer flow and heat transfer in view of the advantage of integrating over a given range within a continuum. Liu et al. [16] utilized distributed order fractional derivatives to investigate boundary layer flow and heat transfer through a moving plate. Qiao et al. [17] solved the pipe flow governing equations of viscoelastic Maxwell fluids with distributed order time fractional derivatives. Long et al. [18] developed the generalized Maxwell and Cattaneo model with distributed order time fractional derivative to study unsteady Marangoni convective boundary layer flow and heat transfer. Yang et al. [19] discussed boundary layer flow and heat transfer by way of the space distributed-order constitution relationship. Feng et al. [20] investigated anomalous transport in a binary medium on finite domains and analyzed the properties of the distributed-order space fractional derivatives with nonlocal operators. Chen et al. [21] presented a study on start-up pipe flow with double time-distributed order Maxwell model. Niu et al. [22] proposed a fast numerical algorithm for the fractional Sobolev model, with non-smooth solutions for the nonlinear distributed-order equations in porous media. Liu et al. [23] constructed a novel distributed order time fractional model to solve heat conduction, anomalous diffusion, and viscoelastic flow problems. Hu et al. [24] applied a distributed order time fractional Maxwell constitutive fluid model to simulate viscoelastic blood flowing in a narrowing blood vessel with a uniform magnetic field. Zhang et al. [25] introduced the distributed-order time fractional derivative to establish the generalized fractional Bloch-Torrey equation in heterogeneous biological tissues.

On the other hand, there are very few studies on natural convective flow and heat transfer in porous media with distributed order time fractional derivatives. This is because the momentum and energy governing equations are strongly coupled, and the analytical solutions are difficult to obtain for

the nonlinear fractional convection terms. Given this, the paper aims to further discuss the internal transport mechanism in natural convective flow and heat transfer of porous media within distributed order time fractional derivative models. The following Section 2 presents unsteady natural convective flow and heat transfer governing equations using the generalized Maxwell model and Darcy's law with initial and boundary conditions. Section 3 presents the fractional finite volume method together with the fractional $L1$ scheme to solve the nonlinear governing equations. A mid-point quadrature rule is employed to discretize the distributed order time fractional derivatives. Section 4 validates the acceptable accuracy of the numerical solutions after the grid independence test and comparisons with exact solutions. Section 5 analyzes and discusses the effects of active physical parameters on velocity and temperature distributions in detail. Section 6 summarizes the main conclusions of this paper.

2. Mathematical formulation

Consider unsteady convective flow and heat transfer of viscoelastic fluid over a vertical plate embedded in a porous medium. The wall temperature is denoted as T_w and is always maintained as a constant. The ambient temperature far away from the plate is T_∞. Particularly, the direction of the vertical plate is selected as the x-axis, while the y-axis is horizontal accordingly. It is assumed that the fluid is incompressible, and the Boussinesq approximation can apply to the external body force. The porous medium is also assumed to be isotropic and homogeneous. Under these assumptions, the momentum conservation equation in the porous medium follows

$$\rho\left(\frac{\partial u}{\partial t}+u\frac{\partial u}{\partial x}+v\frac{\partial u}{\partial y}\right)=\frac{\partial \sigma_{xy}}{\partial y}+g\beta_T\left(T-T_\infty\right)+R, \tag{2.1}$$

where ρ is the fluid constant density, u and v are the corresponding velocity components, σ_{xy} is the shear stress tensor component, g is the acceleration due to gravity, β_T is the thermal expansion coefficient, T is the temperature, and R is the Darcy resistance.

The microscopic structure of the porous medium and associated environments introduce complexity via porosity and permeability. The distributed order fractional derivative provides more flexibility for simulating anomalous diffusion behaviors with multi-scale characteristics [26]. Thus, the generalized distributed order Maxwell model and Darcy's law are developed by integrating the order of the time-fractional derivative, respectively:

$$\sigma_{xy}+\int_0^1 \omega_1(\alpha)\lambda_1^\alpha \frac{\partial^\alpha \sigma_{xy}}{\partial t^\alpha}d\alpha=\mu\frac{\partial u}{\partial y}, \tag{2.2}$$

$$R+\int_0^1 \omega_1(\alpha)\lambda_1^\alpha \frac{\partial^\alpha R}{\partial t^\alpha}d\alpha=-\frac{\mu\varepsilon}{K}u, \tag{2.3}$$

where α is the velocity fractional derivative parameter that characterizes the frequency-dependent complex modulus, λ_1 is the velocity relaxation time, $\omega_1(\alpha)$ is the weight coefficient that follows $\omega_1(\alpha) \geq 0$ and $\int_0^1 \omega_1(\alpha)d\alpha=1$ [27], μ is the dynamic viscosity of the fluid, K and ε are the permeability and

porosity of the porous medium, respectively, and $\frac{\partial^\alpha}{\partial t^\alpha}$ denotes the Caputo fractional derivative operator defined as in (2.4) [28].

$$\frac{\partial^\alpha}{\partial t^\alpha} f(x,y,t) = \frac{1}{\Gamma(m-\alpha)} \int_0^t (t-\eta)^{m-\alpha-1} \frac{\partial f^m(x,y,\eta)}{\partial \eta^m} d\eta \,, m-1 < \alpha < m, \tag{2.4}$$

where $m \in \mathbb{N}^+$, $\Gamma(\cdot)$ denotes the gamma function, and $f(x,y,t)$ is simplified as $f(t)$. Combining Eqs (2.1)–(2.3) to eliminate the terms σ_{xy} and R, the nonlinear coupled momentum equation with distributed order fractional derivative is derived as follows:

$$\begin{aligned} &\frac{\partial u}{\partial t} + \frac{\partial}{\partial x}(uu) + \frac{\partial}{\partial y}(vu) + \int_0^1 \omega_1(\alpha)\lambda_1^\alpha \frac{\partial^{\alpha+1} u}{\partial t^{\alpha+1}} d\alpha + \int_0^1 \omega_1(\alpha)\lambda_1^\alpha \frac{\partial^\alpha}{\partial t^\alpha}\left(\frac{\partial}{\partial x}(uu)\right) d\alpha \\ &+ \int_0^1 \omega_1(\alpha)\lambda_1^\alpha \frac{\partial^\alpha}{\partial t^\alpha}\left(\frac{\partial}{\partial y}(vu)\right) d\alpha = -\frac{\nu_f \varepsilon}{K} u + \nu_f \frac{\partial^2 u}{\partial y^2} + g\beta_T (T - T_\infty) \\ &+ \int_0^1 \omega_1(\alpha)\lambda_1^\alpha \frac{\partial^\alpha}{\partial t^\alpha}\left[g\beta_T (T - T_\infty)\right] d\alpha. \end{aligned} \tag{2.5}$$

Similarly, the homologous energy equation with distributed order fractional derivative is obtained in the following:

$$\begin{aligned} &\frac{\partial T}{\partial t} + \frac{\partial}{\partial x}(uT) + \frac{\partial}{\partial y}(vT) + \int_0^1 \omega_2(\beta)\lambda_2^\beta \frac{\partial^{\beta+1} T}{\partial t^{\beta+1}} d\beta + \int_0^1 \omega_2(\beta)\lambda_2^\beta \frac{\partial^\beta}{\partial t^\beta}\left(\frac{\partial}{\partial x}(uT)\right) d\beta \\ &+ \int_0^1 \omega_2(\beta)\lambda_2^\beta \frac{\partial^\beta}{\partial t^\beta}\left(\frac{\partial}{\partial y}(vT)\right) d\beta = \alpha_f \frac{\partial^2 T}{\partial y^2}, \end{aligned} \tag{2.6}$$

where $\omega_2(\beta)$ denotes the weight coefficient that is suitable for certain conditions as $\omega_2(\beta) \geq 0$ and $\int_0^1 \omega_2(\beta) d\beta = 1$, β is the temperature fractional derivative parameter that improves the efficiency of the thermoelectric material figure-of-merit, λ_2 is the temperature relaxation time, and α_f is the thermal diffusion coefficient.

The initial conditions and boundary conditions of the natural convective flow in the porous medium are assumed as follows:

$$u(x,y,0) = 0, \frac{\partial u(x,y,0)}{\partial t} = 0, \; v(x,y,0) = 0, T(x,y,0) = \begin{cases} T_w, y = 0 \\ T_\infty, y \neq 0 \end{cases}, \; \frac{\partial T(x,y,0)}{\partial t} = 0, u(x,0,t) = 0,$$

$$v(x,0,t) = 0, \; T(x,0,t) = T_w, \; u(0,y,t) = 0, \; T(0,y,t) = T_\infty, \; u(x,\infty,t) = 0, \; T(x,\infty,t) = T_\infty.$$

We employ non-dimensional quantities as follows:

$$x^* = \frac{x}{L}, \quad y^* = \frac{y}{L} Gr^{1/4}, \quad u^* = \frac{uL}{\nu_f} Gr^{-1/2}, \quad v^* = \frac{vL}{\nu_f} Gr^{-1/4}, \quad t^* = \frac{\nu_f t}{L^2} Gr^{1/2}, \quad \lambda_1^* = \frac{\lambda_1 \nu_f}{L^2} Gr^{1/2},$$

$$\lambda_2^* = \frac{\lambda_2 \nu_f}{L^2} Gr^{1/2}, \; Da = \frac{K}{L^2}, Gr = \frac{g\beta_T (T_w - T_\infty) L^3}{\nu_f^2}, \; \theta = \frac{T - T_\infty}{T_w - T_\infty}, \; Pr = \frac{\nu_f}{\alpha_f},$$

where L is the total length of the plate, Da is the Darcy number, Gr is the Grashof number, and Pr is the Prandtl number.

Non-dimensional distributed order governing equations for the porous medium are derived with time-fractional derivatives after omitting the dimensionless sign "*":

$$\frac{\partial u}{\partial x}+\frac{\partial v}{\partial y}=0, \tag{2.7}$$

$$\begin{aligned}&\frac{\partial u}{\partial t}+\frac{\partial}{\partial x}(uu)+\frac{\partial}{\partial y}(vu)+\int_0^1\omega_1(\alpha)\lambda_1^{\alpha}\frac{\partial^{\alpha+1}u}{\partial t^{\alpha+1}}d\alpha+\int_0^1\omega_1(\alpha)\lambda_1^{\alpha}\frac{\partial^{\alpha}}{\partial t^{\alpha}}\left(\frac{\partial}{\partial x}(uu)\right)d\alpha\\&+\int_0^1\omega_1(\alpha)\lambda_1^{\alpha}\frac{\partial^{\alpha}}{\partial t^{\alpha}}\left(\frac{\partial}{\partial y}(vu)\right)d\alpha=-\frac{\varepsilon u}{DaGr^{1/2}}+\frac{\partial^2 u}{\partial y^2}+\theta+\int_0^1\omega_1(\alpha)\lambda_1^{\alpha}\frac{\partial^{\alpha}\theta}{\partial t^{\alpha}}d\alpha,\end{aligned} \tag{2.8}$$

$$\begin{aligned}&\frac{\partial \theta}{\partial t}+\frac{\partial}{\partial x}(u\theta)+\frac{\partial}{\partial y}(v\theta)+\int_0^1\omega_2(\beta)\lambda_2^{\beta}\frac{\partial^{\beta+1}\theta}{\partial t^{\beta+1}}d\beta+\int_0^1\omega_2(\beta)\lambda_2^{\beta}\frac{\partial^{\beta}}{\partial t^{\beta}}\left(\frac{\partial}{\partial x}(u\theta)\right)d\beta\\&+\int_0^1\omega_2(\beta)\lambda_2^{\beta}\frac{\partial^{\beta}}{\partial t^{\beta}}\left(\frac{\partial}{\partial y}(v\theta)\right)d\beta=\frac{1}{Pr}\frac{\partial^2\theta}{\partial y^2}.\end{aligned} \tag{2.9}$$

The non-dimensional initial conditions and boundary conditions are subject to

$$u(x,y,0)=0,\ \frac{\partial u(x,y,0)}{\partial t}=0,\ v(x,y,0)=0,\ \theta(x,y,0)=\begin{cases}1, y=0\\0, y\neq 0\end{cases},\ \frac{\partial\theta(x,y,0)}{\partial t}=0,\ u(x,0,t)=0,$$

$$v(x,0,t)=0,\ \theta(x,0,t)=1,\ u(0,y,t)=0,\ \theta(0,y,t)=0,\ u(x,\infty,t)=0,\ \theta(x,\infty,t)=0.$$

3. Numerical technique

Figure 1 shows the collocated grid system of the physical problem, where the computational domain is divided into discrete control volumes, and the general central nodal point is denoted as PP. The grid distances between the inner nodes in the x and y directions are denoted as Δx and Δy, respectively. The time step is denoted as Δt.

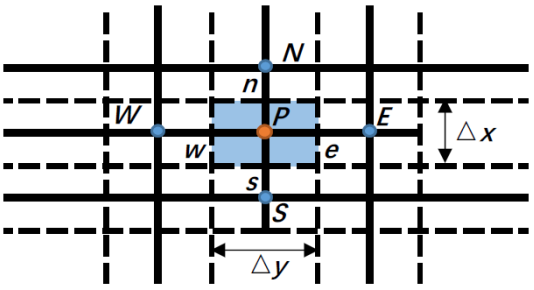

Figure 1. The grid system of the control volume.

First, the following integral equation is derived by the integration of Eq (2.9):

$$\begin{aligned}&\int_t^{t+\Delta t}\int_{\Delta V}\frac{\partial\theta}{\partial t}dVdt+\int_t^{t+\Delta t}\int_{\Delta V}\frac{\partial}{\partial x}(u\theta)dVdt+\int_t^{t+\Delta t}\int_{\Delta V}\frac{\partial}{\partial y}(v\theta)dVdt\\&+\int_t^{t+\Delta t}\int_{\Delta V}\int_0^1\omega_2(\beta)\lambda_2^{\beta}\frac{\partial^{\beta+1}\theta}{\partial t^{\beta+1}}d\beta dVdt+\int_t^{t+\Delta t}\int_{\Delta V}\int_0^1\omega_2(\beta)\lambda_2^{\beta}\frac{\partial^{\beta}}{\partial t^{\beta}}\left(\frac{\partial}{\partial x}(u\theta)\right)d\beta dVdt\\&+\int_t^{t+\Delta t}\int_{\Delta V}\int_0^1\omega_2(\beta)\lambda_2^{\beta}\frac{\partial^{\beta}}{\partial t^{\beta}}\left(\frac{\partial}{\partial y}(v\theta)\right)d\beta dVdt=\int_t^{t+\Delta t}\int_{\Delta V}\frac{1}{Pr}\frac{\partial^2\theta}{\partial y^2}dVdt,\end{aligned}\tag{3.1}$$

where ΔV is the control volume that equals $\Delta x\cdot\Delta y$.

The backward difference scheme is implemented to discretize the first item of the time term in Eq (3.1) as follows:

$$\int_t^{t+\Delta t}\int_{\Delta V}\frac{\partial\theta}{\partial t}dVdt=\left(\theta_P^k-\theta_P^{k-1}\right)\cdot\Delta V+O(\Delta t).\tag{3.2}$$

The volume integrals inside the convective terms and diffusive term are substituted by surface integrals, which are carried out by the first-order upwind difference scheme. In addition, the gradient at the interface is approximated by the central difference format. After these methods of processing, the following discretized equations of integer derivatives are formulated:

$$\begin{aligned}&\int_t^{t+\Delta t}\int_{\Delta V}\frac{\partial}{\partial x}(u\theta)dVdt=\left[\left(uA\theta\right)_n^k-\left(uA\theta\right)_s^k\right]\cdot\Delta t\\&=\left(u_P^{k-1}A_n\theta_P^k-u_S^{k-1}A_s\theta_S^k\right)\cdot\Delta t+O(\Delta x),\end{aligned}\tag{3.3}$$

$$\begin{aligned}&\int_t^{t+\Delta t}\int_{\Delta V}\frac{\partial}{\partial y}(v\theta)dVdt=\left[\left(vA\theta\right)_e^k-\left(vA\theta\right)_w^k\right]\cdot\Delta t\\&=\left(v_E^{k-1}A_e\theta_E^k-v_P^{k-1}A_w\theta_P^k\right)\cdot\Delta t+O(\Delta y),\end{aligned}\tag{3.4}$$

$$\begin{aligned}&\int_t^{t+\Delta t}\int_{\Delta V}\frac{\partial^2\theta}{\partial y^2}dVdt=\left[\left(A\frac{\partial\theta}{\partial y}\right)_e^k-\left(A\frac{\partial\theta}{\partial y}\right)_w^k\right]\cdot\Delta t\\&=\left(A_e\frac{\theta_E^k-\theta_P^k}{\Delta y}-A_w\frac{\theta_P^k-\theta_W^k}{\Delta y}\right)\cdot\Delta t+O(\Delta y^2),\end{aligned}\tag{3.5}$$

where A represents the face area of the control volume, and $A_w = A_e = \Delta x$, $A_n = A_s = \Delta y$.

Second, the mid-point quadrature rule is adopted to approximate the distributed order time fractional derivatives. Distributed-order fractional partial differential equations (PDEs) can be regarded as the limiting case of multi-term fractional PDEs [29]. Diethelm and Ford [30] have observed that small changes in the order of a fractional PDE lead to only slight changes in the final solution, which gives initial support to the employed numerical integration method. Thus, the summations of multi-fractional terms are acquired [31]:

$$\int_0^1 \omega_2(\beta)\lambda_2^{\beta}\frac{\partial^{\beta+1}\theta}{\partial t^{\beta+1}}d\beta \approx h_\beta \sum_{s=1}^{K}\omega_2(\beta_s)\lambda_2^{\beta_s}\frac{\partial^{\beta_s+1}\theta}{\partial t^{\beta_s+1}}, \tag{3.6}$$

$$\int_0^1 \omega_2(\beta)\lambda_2^{\beta}\frac{\partial^{\beta}}{\partial t^{\beta}}\left(\frac{\partial}{\partial x}(u\theta)\right)d\beta \approx h_\beta \sum_{s=1}^{K}\omega_2(\beta_s)\lambda_2^{\beta_s}\frac{\partial^{\beta_s}}{\partial t^{\beta_s}}\left(\frac{\partial}{\partial x}(u\theta)\right), \tag{3.7}$$

$$\int_0^1 \omega_2(\beta)\lambda_2^{\beta}\frac{\partial^{\beta}}{\partial t^{\beta}}\left(\frac{\partial}{\partial y}(v\theta)\right)d\beta \approx h_\beta \sum_{s=1}^{K}\omega_2(\beta_s)\lambda_2^{\beta_s}\frac{\partial^{\beta_s}}{\partial t^{\beta_s}}\left(\frac{\partial}{\partial y}(v\theta)\right), \tag{3.8}$$

where $h_\beta = \frac{1}{K}$ denotes the fractional parameter step, and $\beta_s = \frac{(s-1)h_\beta + sh_\beta}{2}$.

The fractional $L1$ scheme is adopted to estimate the time-fractional derivative of order β_s, as $0 < \beta_s < 1$ [32, 33] under the assumption that $f(t_k) \in C^2[0,t]$:

$$\frac{\partial^{\beta_s}}{\partial t^{\beta_s}}f(t_k) = \frac{\Delta t^{-\beta_s}}{\Gamma(2-\beta_s)}\left[f(t_k) - \beta_{k-1}^{s}f(t_0) - \sum_{j=1}^{k-1}\left(\beta_{j-1}^{s} - \beta_j^{s}\right)f(t_{k-j})\right] + O\left(\Delta t^{2-\beta_s}\right), \tag{3.9}$$

where $\beta_j^s = (j+1)^{1-\beta_s} - j^{1-\beta_s}$. For the order of β_s+1, the Caputo time fractional derivative has the following property [28]:

$$\frac{\partial^{\beta_s+1}}{\partial t^{\beta_s+1}}f(t_k) = \frac{\partial^{\beta_s}}{\partial t^{\beta_s}}f'(t_k), \tag{3.10}$$

where $f'(t_k) = \left[f(t_k) - f(t_{k-1})\right]/\Delta t$.

Utilizing Eqs (3.9) and (3.10), Eqs (3.6)–(3.8) can be transformed into the discretized forms

$$\begin{aligned}&\int_0^1 \omega_2(\beta)\lambda_2^{\beta}\frac{\partial^{\beta+1}\theta}{\partial t^{\beta+1}}d\beta \\ &= h_\beta \Delta V \sum_{s=1}^{K}\omega_2(\beta_s)\frac{\lambda_2^{\beta_s}\cdot\Delta t^{-\beta_s}}{\Gamma(2-\beta_s)}\left[\theta_P^k - \theta_P^{k-1} - \sum_{j=1}^{k-1}\left(\beta_{j-1}^{s} - \beta_j^{s}\right)\left(\theta_P^{k-j} - \theta_P^{k-j-1}\right)\right] + R_1,\end{aligned} \tag{3.11}$$

$$\begin{aligned}&\int_0^1 \omega_2(\beta)\lambda_2^{\beta}\frac{\partial^{\beta}}{\partial t^{\beta}}\left(\frac{\partial}{\partial x}(u\theta)\right)d\beta = h_\beta \sum_{s=1}^{K}\omega_2(\beta_s)\frac{\lambda_2^{\beta_s}\cdot\Delta t^{-\beta_s+1}}{\Gamma(2-\beta_s)}\cdot \\ &\left[u_P^{k-1}A_n\theta_P^k - u_S^{k-1}A_s\theta_S^k - \sum_{j=1}^{k-1}\left(\beta_{j-1}^{s} - \beta_j^{s}\right)\left(u_P^{k-j-1}A_n\theta_P^{k-j} - u_S^{k-j-1}A_s\theta_S^{k-j}\right)\right] + R_2,\end{aligned} \tag{3.12}$$

$$\int_0^1 \omega_2(\beta)\lambda_2^{\beta}\frac{\partial^{\beta}}{\partial t^{\beta}}\left(\frac{\partial}{\partial y}(v\theta)\right)d\beta = h_{\beta}\sum_{s=1}^{K}\omega_2(\beta_s)\frac{\lambda_2^{\beta_s}\cdot\Delta t^{-\beta_s+1}}{\Gamma(2-\beta_s)}\cdot$$
$$\left[v_E^{k-1}A_e\theta_E^k - v_P^{k-1}A_w\theta_P^k - \sum_{j=1}^{k-1}\left(\beta_{j-1}^s-\beta_j^s\right)\left(v_E^{k-j-1}A_e\theta_E^{k-j} - v_P^{k-j-1}A_w\theta_P^{k-j}\right)\right] + R_3, \tag{3.14}$$

where the truncation errors are $R_1 \le C(\Delta t)$, $R_2 \le C(\Delta t+\Delta x)$, $R_3 \le C(\Delta t+\Delta y)$.

Finally, the iterative difference equation of Eq (2.9) is established:

$$a_P\theta_P^k = a_S\theta_S^k + a_W\theta_W^k + a_E\theta_E^k + S_P, \tag{3.15}$$

$$a_P = \left(1+\sum_{s=1}^{K}r_s\right)\cdot\left(\frac{\Delta V}{\Delta t}+\Delta y\cdot u_P^{k-1}-\Delta x\cdot v_P^{k-1}\right)+\frac{2\Delta x}{Pr\cdot\Delta y},$$

$$a_S = \left(1+\sum_{s=1}^{K}r_s\right)\cdot\Delta y\cdot u_S^{k-1},\quad a_w = \frac{\Delta x}{Pr\cdot\Delta y},\quad a_E = \frac{\Delta x}{Pr\cdot\Delta y}-\left(1+\sum_{s=1}^{K}r_s\right)\cdot\Delta x\cdot v_E^{k-1},$$

$$S_P = \left(1+\sum_{s=1}^{K}r_s\right)\cdot\frac{\Delta V}{\Delta t}\cdot\theta_P^{k-1}+\frac{\Delta V}{\Delta t}\cdot\sum_{s=1}^{K}r_s\sum_{j=1}^{k-1}\left(\beta_{j-1}^s-\beta_j^s\right)\left(\theta_P^{k-j}-\theta_P^{k-j-1}\right)$$
$$+\Delta y\cdot\sum_{s=1}^{K}r_s\sum_{j=1}^{k-1}\left(\beta_{j-1}^s-\beta_j^s\right)\left(u_P^{k-j-1}\theta_P^{k-j}-u_S^{k-j-1}\theta_S^{k-j}\right)$$
$$+\Delta x\cdot\sum_{s=1}^{K}r_s\sum_{j=1}^{k-1}\left(\beta_{j-1}^s-\beta_j^s\right)\left(v_E^{k-j-1}\theta_E^{k-j}-v_P^{k-j-1}\theta_P^{k-j}\right),$$

where $r_s = h_{\beta}\omega_2(\beta_s)\frac{\lambda_2^{\beta_s}\cdot\Delta t^{-\beta_s}}{\Gamma(2-\beta_s)}$.

The velocity terms of Eq (2.8) are carried out to deduce the discretized forms similarly. The semi-implicit scheme is utilized for the integration of the single velocity and temperature terms:

$$\int_t^{t+\Delta t}\int_{\Delta V} u dV dt = \frac{\Delta t\cdot\Delta V}{2}\left(u_P^k+u_P^{k-1}\right)+O(\Delta t), \tag{3.16}$$

$$\int_t^{t+\Delta t}\int_{\Delta V} \theta dV dt = \frac{\Delta t\cdot\Delta V}{2}\left(\theta_P^k+\theta_P^{k-1}\right)+O(\Delta t), \tag{3.17}$$

$$\int_t^{t+\Delta t}\int_{\Delta V}\int_0^1 \omega_1(\alpha)\lambda_1^{\alpha}\frac{\partial^{\alpha}\theta}{\partial t^{\alpha}}d\alpha dV dt \approx \frac{h_{\alpha}\Delta V}{2}\sum_{s=1}^{K}\omega_1(\alpha_s)\frac{\lambda_1^{\alpha_s}\cdot\Delta t^{-\alpha_s+1}}{\Gamma(2-\alpha_s)}\cdot$$
$$\left[\theta_P^k+\theta_P^{k-1}-\sum_{j=1}^{k-1}\left(\alpha_{j-1}^s-\alpha_j^s\right)\left(\theta_P^{k-j}+\theta_P^{k-j-1}\right)\right]+O(\Delta t), \tag{3.18}$$

where $h_\alpha = \frac{1}{K}$, $\alpha_s = \frac{(s-1)h_\alpha + sh_\alpha}{2}$, $\alpha_j^s = (j+1)^{1-\alpha_s} - j^{1-\alpha_s}$.

Meanwhile, Eq (2.7) is integrated to obtain the velocity component in the *y* direction as follows:

$$\begin{aligned} 0 &= \int_t^{t+\Delta t}\int_{\Delta V}\frac{\partial u}{\partial x}\,dVdt + \int_t^{t+\Delta t}\int_{\Delta V}\frac{\partial v}{\partial y}\,dVdt \\ &= \frac{\Delta t}{2}\left[(uA)_n^k - (uA)_s^k + (uA)_n^{k-1} - (uA)_s^{k-1}\right] + \frac{\Delta t}{2}\left[(vA)_e^k - (vA)_w^k + (vA)_e^{k-1} - (vA)_w^{k-1}\right], \end{aligned} \tag{3.19}$$

$$v_P^k = -v_P^{k-1} + v_W^k + v_W^{k-1} - \frac{\Delta y}{\Delta x}\left(u_P^k - u_S^k + u_P^{k-1} - u_S^{k-1}\right) + O(\Delta x + \Delta y). \tag{3.20}$$

4. Validation of the numerical results

4.1. Solvability of the iterative difference equation

Theorem 1. *The iterative difference equation (3.14) is uniquely solvable.*
Proof. The values of θ at the kth time level are acquired from the iterative difference equation (3.14). We summarize the difference scheme on a particular *i*-level in matrix form:

$$G_i\theta_i^k = H_i\theta_i^{k-1} + S_i^k, \tag{4.1}$$

$$\theta_i^k = \left[\theta_{i,2}^k, \theta_{i,3}^k, \cdots, \theta_{i,j}^k, \cdots, \theta_{i,N-1}^k\right]^T,\ \theta_i^{k-1} = \left[\theta_{i,2}^{k-1}, \theta_{i,3}^{k-1}, \cdots, \theta_{i,j}^{k-1}, \cdots, \theta_{i,N-1}^{k-1}\right]^T,$$

$$G_i = \begin{pmatrix} a_P(i,2) & -a_E(i,3) & \cdots & \cdots & \cdots & \cdots & 0 \\ 0 & \cdots & -a_w(i,j-1) & a_P(i,j) & -a_E(i,j+1) & \cdots & 0 \\ 0 & \cdots & \cdots & \cdots & \cdots & -a_W(i,N-2) & a_P(i,N-1) \end{pmatrix},$$

$$H_i = \left[a_s(i,2), a_s(i,3), \cdots, a_s(i,j), \cdots, a_s(i,N-1)\right]^T,$$

$$S_i^k = \left[S_P(i,2) + a_W(i,2)\theta_{i,1}^k, S_P(i,3), \cdots, S_P(i,j), \cdots, S_P(i,N-1) + a_E(i,N)\theta_{i,N}^k\right]^T,$$

where G_i is a tri-diagonal and full-rank matrix.

Therefore, the difference scheme (3.20) is uniquely solvable. The numerical solutions of u_i^k and v_i^k are similarly proved.

□

4.2. Grid independence verification

The computational domain is regarded as a rectangle with sides X_{max} =1 and Y_{max} = 12, respectively, where Y_{max} represents y→∞ approximately. The coordinate mesh sizes are fixed as Δ*x*

= 0.05 and $\Delta y = 0.1$, respectively, and the time step is selected as $\Delta t = 0.1$. To compromise between numerical precision and computation time, the absolute differences between two consecutive time steps are set as smaller than 10^{-3} within the whole domain. To measure the grid independence, Figure 2 presents the numerical solutions through different groups of grid systems. The velocity curves are in good coincidence, which demonstrates that the selected mesh sizes are appropriate for the calculations.

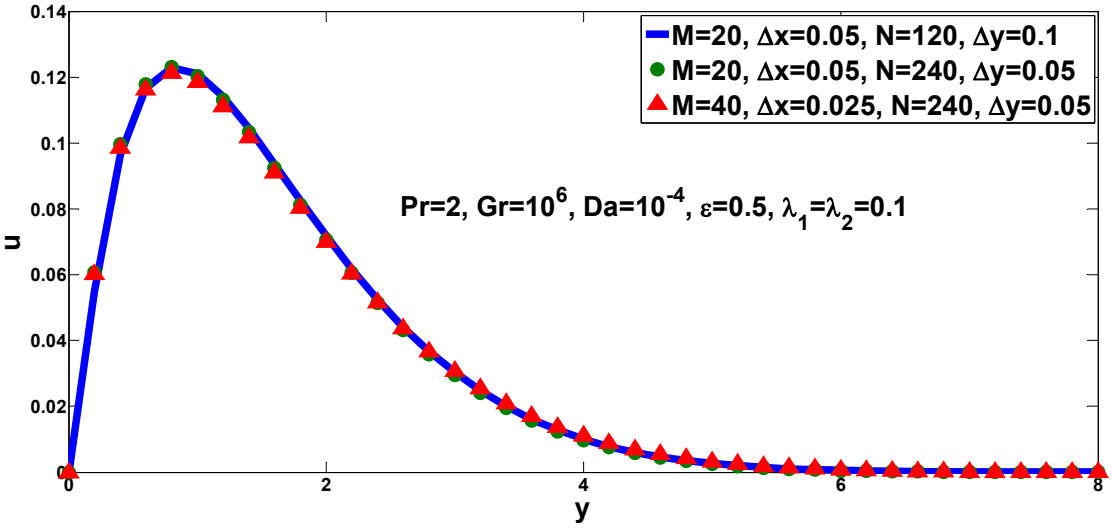

Figure 2. Grid independence test.

4.3. Numerical test with source terms

To verify the numerical error accuracy of the presented fractional finite volume method, comparisons are implemented between numerical solutions and exact solutions with two source terms:

$$\begin{aligned}&\frac{\partial u}{\partial t}+\frac{\partial}{\partial x}(uu)+\frac{\partial}{\partial y}(vu)+\int_0^1\omega_1(\alpha)\lambda_1^{\alpha}\frac{\partial^{\alpha+1}u}{\partial t^{\alpha+1}}d\alpha+\int_0^1\omega_1(\alpha)\lambda_1^{\alpha}\frac{\partial^{\alpha}}{\partial t^{\alpha}}\left(\frac{\partial}{\partial x}(uu)\right)d\alpha\\&+\int_0^1\omega_1(\alpha)\lambda_1^{\alpha}\frac{\partial^{\alpha}}{\partial t^{\alpha}}\left(\frac{\partial}{\partial y}(vu)\right)d\alpha=-\frac{\varepsilon u}{DaGr^{1/2}}+\frac{\partial^2 u}{\partial y^2}+\theta+\int_0^1\omega_1(\alpha)\lambda_1^{\alpha}\frac{\partial^{\alpha}\theta}{\partial t^{\alpha}}d\alpha+f_1(x,y,t),\end{aligned}\tag{4.12}$$

$$\begin{aligned}&\frac{\partial\theta}{\partial t}+\frac{\partial}{\partial x}(u\theta)+\frac{\partial}{\partial y}(v\theta)+\int_0^1\omega_2(\beta)\lambda_2^{\beta}\frac{\partial^{\beta+1}\theta}{\partial t^{\beta+1}}d\beta+\int_0^1\omega_2(\beta)\lambda_2^{\beta}\frac{\partial^{\beta}}{\partial t^{\beta}}\left(\frac{\partial}{\partial x}(u\theta)\right)d\beta\\&+\int_0^1\omega_2(\beta)\lambda_2^{\beta}\frac{\partial^{\beta}}{\partial t^{\beta}}\left(\frac{\partial}{\partial y}(v\theta)\right)d\beta=\frac{1}{Pr}\frac{\partial^2\theta}{\partial y^2}+f_2(x,y,t).\end{aligned}\tag{4.13}$$

The homogeneous initial conditions and boundary conditions are given as follows:

$$u(x,y,0)=0,\frac{\partial u(x,y,0)}{\partial t}=0,\ v(x,y,0)=0,\theta(x,y,0)=0,\ \frac{\partial\theta(x,y,0)}{\partial t}=0,u(x,0,t)=0,$$

$$v(x,0,t)=0,\ \theta(x,0,t)=0,\ u(0,y,t)=0,\ \theta(0,y,t)=0,\ u(x,1,t)=0,\ \theta(x,1,t)=0.$$

The eligible exact solutions are chosen specially as

$$u(x,y,t)=x^2(1-x)^2\,y^2(1-y)^2\,t^2,$$

$$v(x,y,t)=-2x(1-x)(1-2x)\left(\frac{1}{3}y^3-\frac{1}{2}y^4+\frac{1}{5}y^5\right)t^2,$$

$$\theta(x,y,t)=x^2(1-x)^2\,y^2(1-y)^2\,t^2.$$

The two source terms are constructed by reverse derivation:

$$f_1(x,y,t)=$$
$$\left[\int_0^1\omega_1(\alpha)\frac{2\lambda_1^{\alpha}t^{1-\alpha}}{\Gamma(2-\alpha)}d\alpha+2t-\int_0^1\omega_1(\alpha)\frac{2\lambda_1^{\alpha}t^{2-\alpha}}{\Gamma(3-\alpha)}d\alpha-t^2\right]x^2(1-x)^2\,y^2(1-y)^2$$
$$+\left(\int_0^1\omega_1(\alpha)\frac{24\lambda_1^{\alpha}t^{4-\alpha}}{\Gamma(5-\alpha)}d\alpha+t^4\right)\left[(1-x)^3(2x^3-4x^4)(y^4-y^5)\left(\frac{1}{3}-\frac{2}{3}y+\frac{3}{5}y^2-\frac{1}{5}y^3\right)\right]$$
$$-2x^2(1-x)^2(1-6y+6y^2)t^2+\frac{\varepsilon x^2(1-x)^2\,y^2(1-y)^2\,t^2}{DaGr^{1/2}},$$

$$f_2(x,y,t)=$$
$$\left[\int_0^1\omega_2(\beta)\frac{\lambda_2^{\beta}t^{1-\beta}}{\Gamma(2-\beta)}d\beta+t\right]2x^2(1-x)^2\,y^2(1-y)^2-\frac{2}{\mathrm{Pr}}x^2(1-x)^2(1-6y+6y^2)t^2$$
$$+\left(\int_0^1\omega_2(\beta)\frac{24\lambda_2^{\beta}t^{4-\beta}}{\Gamma(5-\beta)}d\beta+t^4\right)\left[(1-x)^3(2x^3-4x^4)(y^4-y^5)\left(\frac{1}{3}-\frac{2}{3}y+\frac{3}{5}y^2-\frac{1}{5}y^3\right)\right].$$

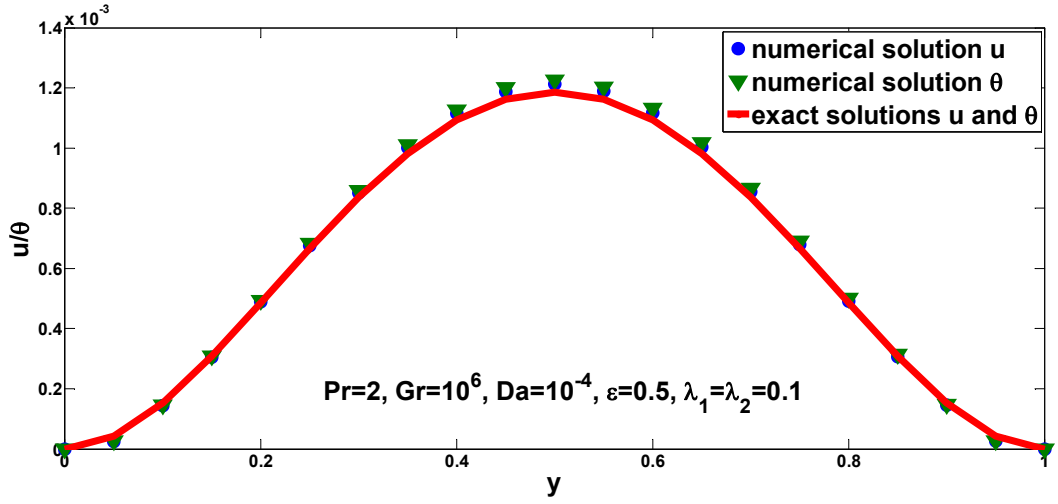

Figure 3. Comparison between numerical solutions and exact solutions.

Figure 3 illustrates the comparisons between the exact solutions and numerical solutions of u and θ. The velocity and temperature distributions are both in fine consistency, which verifies that the presented fractional finite volume method has reliable convergence accuracy.

5. Results and discussion

In this section, the effects of the active physical parameters on velocity and temperature distributions are illustrated graphically: namely, the porosity, Darcy number, and the relaxation time parameters. The distributed order fractional derivatives are integrated over a given range [0,1], and the summations of multi-fractional terms are acquired by the mid-point quadrature rule in Eqs (3.6)–(3.8). For this reason, the effects of the fractional derivative parameters are not discussed in this paper. The Prandtl number and Grashof number are both fixed as constants for brevity.

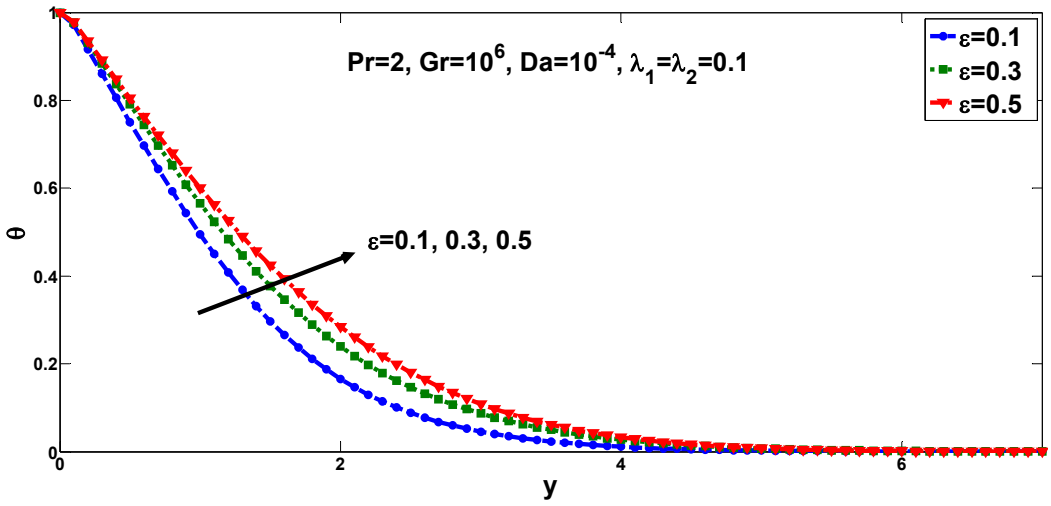

Figure 4. Temperature profiles with different ε.

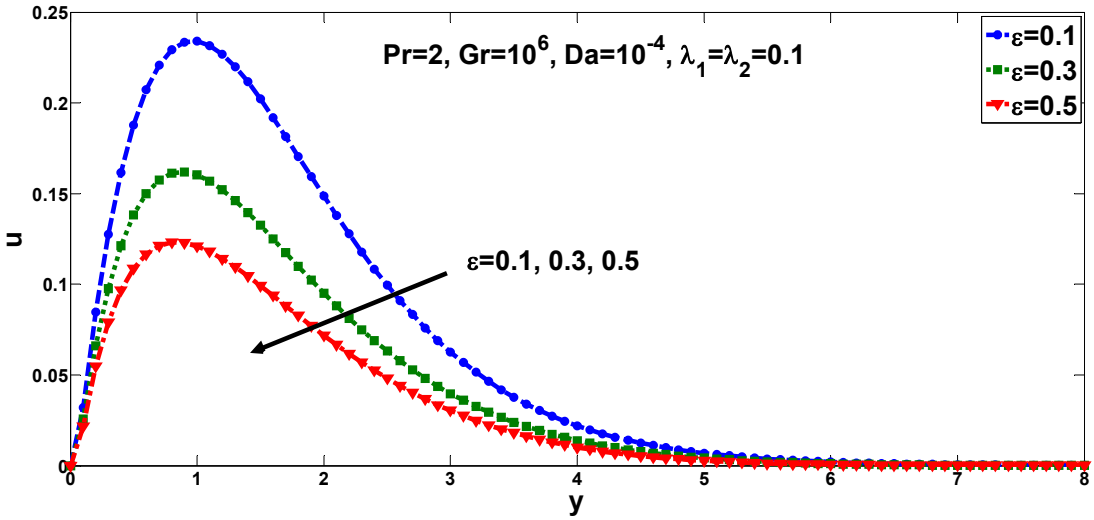

Figure 5. Velocity profiles with different ε.

Figure 4 shows temperature profiles with different values of porosity. The temperature distribution is monotone decreasing for a single value of porosity. With the increase of ε, the temperature distribution increases, and the thickness of the thermal boundary layer gets bigger. The velocity profiles with different ε are depicted in Figure 5. Each velocity profile is not monotone and

possesses a maximum value. As the porosity increases, the velocity distribution declines, and the velocity boundary layer becomes thinner. In addition, the point location of the maximum value gets closer to the vertical plate. These results demonstrate that larger porosity imposes negative restrictions on momentum transfer.

The effects of Darcy number on temperature and velocity profiles are illustrated in Figures 6 and 7. It is found in Figure 6 that the temperature distribution shifts down with the increase of *Da*, but the thickness of the temperature boundary layer declines slightly. In Figure 7, the velocity distribution rises with the increase of *Da*, but the increasing magnitude lessens distinctly. The result proves that the permeability accelerates the development of the velocity. It can be concluded that the porosity and permeability have opposite influences on temperature and velocity fields.

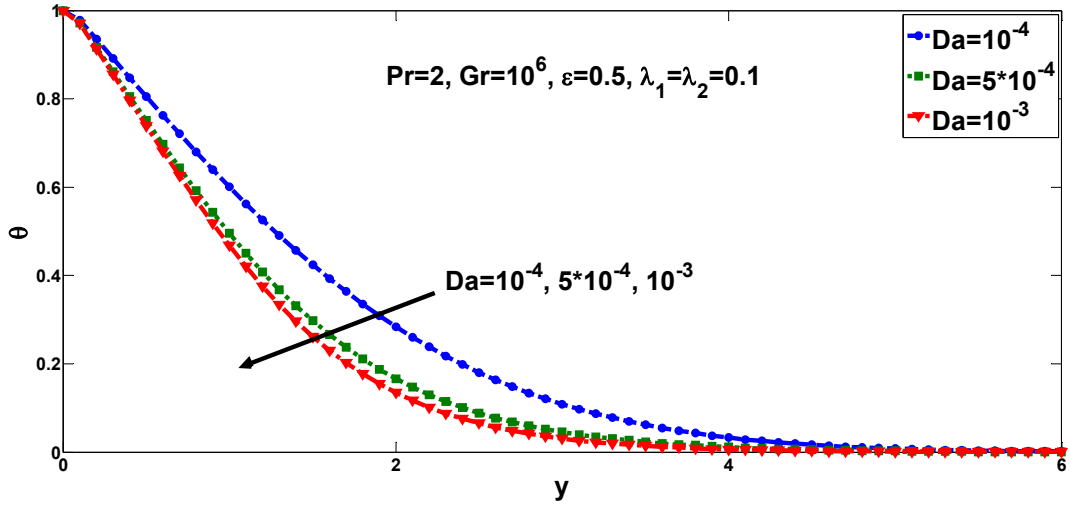

Figure 6. Temperature profiles with different Da.

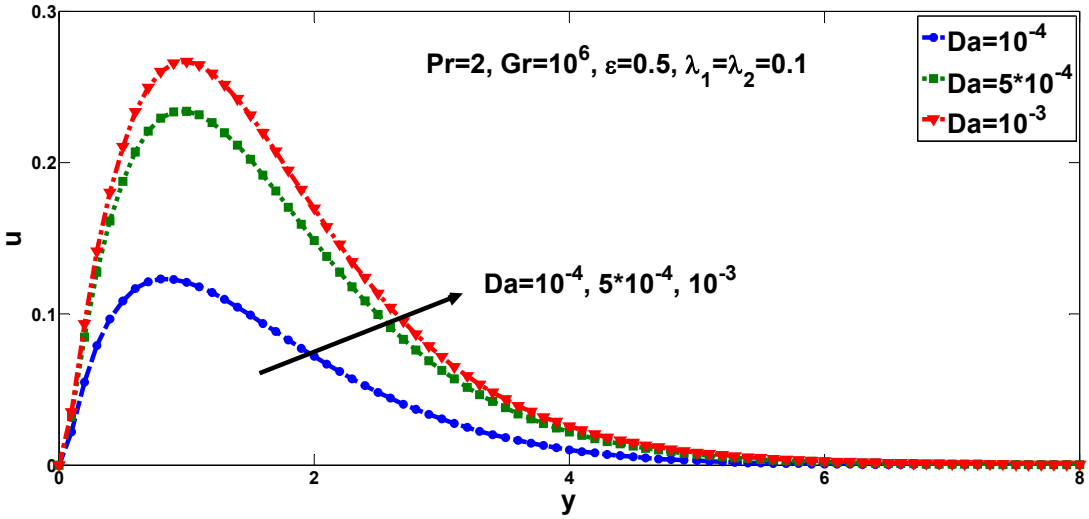

Figure 7. Velocity profiles with different Da.

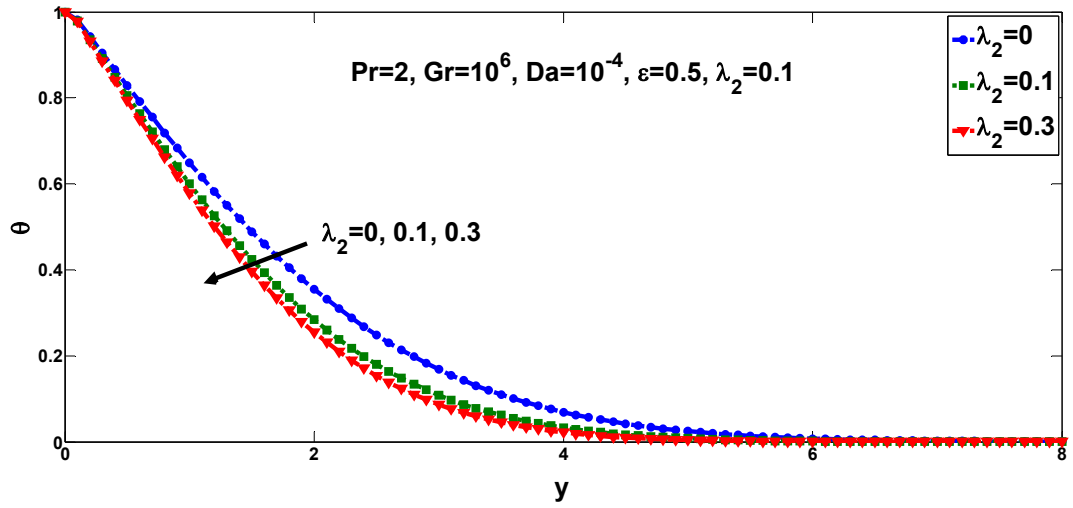

Figure 8. Temperature profiles with different λ_2.

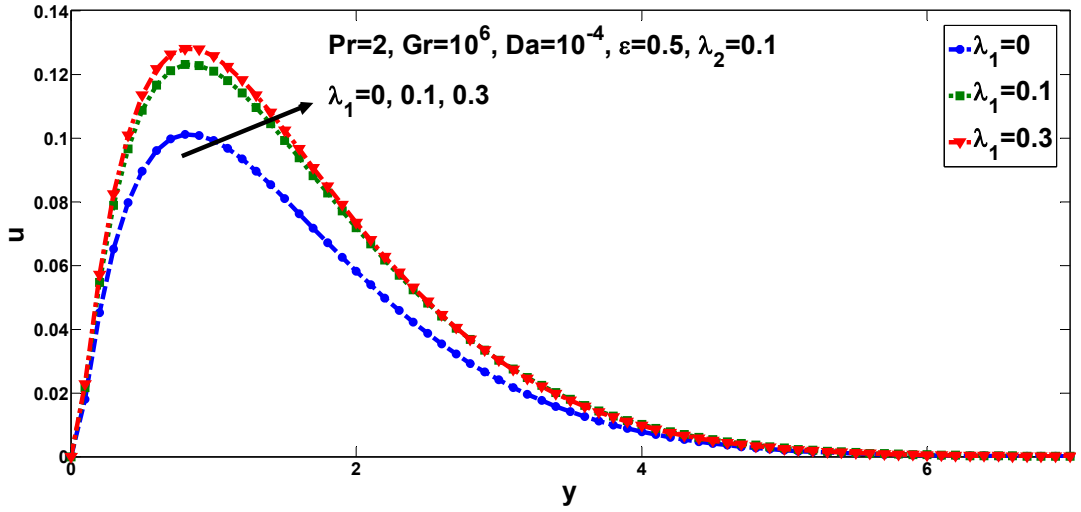

Figure 9. Velocity profiles with different λ_1.

Figures 8–10 present the effects of the relaxation time λ_1 and λ_2 on velocity and temperature. It can be seen from Figure 8 that the temperature distribution decreases apparently with the increase of λ_2. In Figure 9, the velocity distribution rises as the relaxation time λ_1 increases, where the Newtonian fluid that responds to $\lambda_1 = 0$ has the smallest velocity values. The result verifies that the velocity relaxation time promotes the momentum transfer. In Figure 10, the velocity distribution descends with the augment of λ_2, which has inverse effects compared with the relaxation time λ_1. The velocity profiles stay close to each other near the plate and separate evidently at a certain distance from the plate. Meanwhile, the velocity boundary layer thickness reduces slightly with the increase of λ_2.

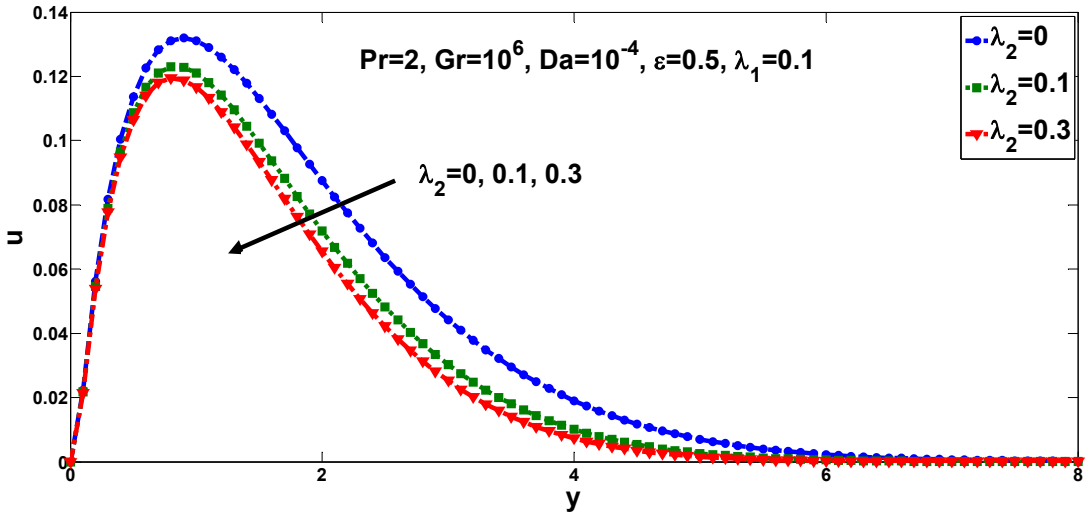

Figure 10. Velocity profiles with different λ_2.

6. Conclusions

This paper discussed the unsteady natural convective flow and heat transfer of generalized Maxwell viscoelastic fluids with distributed order time fractional derivatives embedded in a porous medium. The finite volume method combined with the fractional $L1$ scheme rule was applied to solve the nonlinear governing equations. Numerical solutions of velocity and temperature were discussed after the grid independence test and comparisons with exact solutions. Results are concluded as follows: (i). The temperature distribution rises with the increase of ε but declines as Da and λ_2 become larger. (ii). The velocity distribution ascends with the augment of Da and λ_1 but reduces with the increase of ε and λ_2.

Acknowledgments

The work is supported by the Outstanding Youth Research Project of Anhui Universities (2023AH030075), the National Natural Science Foundations of China (No. 12102093), the Natural Science Research Project of Anhui Universities (2022AH051336), the Talent Project of Fuyang Normal University (rcxm202105).

Use of AI tools declaration

The authors declare that they have not used artificial intelligence (AI) tools in the creation of this article.

Conflict of interest

The author declares that he has no conflict of interest.

References

1. B. Khuzhayorov, J. L. Auriault, P. Royer, Derivation of macroscopic filtration law for transient linear viscoelastic fluid flow in porous media, *Int. J. Eng. Sci.*, **38** (2000), 487–504. https://doi.org/10.1016/S0020-7225(99)00048-8
2. M. S. Malashetty, I. S. Shivakumara, S. Kulkarni, M. Swamy, Convective instability of Oldroyd-B fluid saturated porous layer heated from below using a thermal non-equilibrium model, *Transp Porous Med*, **64** (2006), 123–139. https://doi.org/10.1007/s11242-005-1893-0
3. I. S. Shivakumara, M. Dhananjaya, C. O Ng, Thermal convective instability in an Oldroyd-B nanofluid saturated porous layer, *Int J Heat Mass Tran*, **84** (2015), 167–177. https://doi.org/10.1016/j.ijheatmasstransfer.2015.01.010
4. H. Xu, X. Jiang, Creep constitutive models for viscoelastic materials based on fractional derivatives, *Comput. Math. Appl.*, **73** (2017), 1377–1384. https://doi.org/10.1016/j.camwa.2016.05.002
5. D. Yao, A fractional dashpot for nonlinear viscoelastic fluids, *J. Rheol.*, **62** (2018), 619–629. https://doi.org/10.1122/1.5012504
6. M. Shen, L. Chen, M. Zhang, F. Liu, A renovated Buongiorno's model for unsteady Sisko nanofluid with fractional Cattaneo heat flux, *Int J Heat Mass Tran.*, 126 (2018), 277–286. https://doi.org/10.1016/j.ijheatmasstransfer.2018.05.131
7. X. Chen, W. Yang, X. Zhang, F. Liu, Unsteady boundary layer flow of viscoelastic MHD fluid with a double fractional Maxwell model, *Appl. Math. Lett.*, **95** (2019), 143–149. https://doi.org/10.1016/j.aml.2019.03.036
8. Q. Wei, H. W. Zhou, S. Yang, Non-Darcy flow models in porous media via Atangana-Baleanu derivative, *Chaos Soliton Fract*, **141** (2020), 110335. https://doi.org/10.1016/j.chaos.2020.110335
9. X. Yang, Y. J. Liang, W. Chen, Anomalous imbibition of non-Newtonian fluids in porous media, *Chem. Eng. Sci.*, **211** (2020), 115265. https://doi.org/10.1016/j.ces.2019.115265
10. S. E. Ahmed, Caputo fractional convective flow in an inclined wavy vented cavity filled with a porous medium using Al_2O_3-Cu hybrid nanofluids, *Int. Commun. Heat Mass Transf.*, **116** (2020), 104690. https://doi.org/10.1016/j.icheatmasstransfer.2020.104690
11. Z. Y. Ai, Y. Z. Zhao, W. J. Liu, Fractional derivative modeling for axisymmetric consolidation of multilayered cross-anisotropic viscoelastic porous media, *Comput. Math. Appl.*, **79** (2020), 1321–1334. https://doi.org/10.1016/j.camwa.2019.08.033
12. X. Y. Jiang, H. Zhang, S. W. Wang, Unsteady magnetohydrodynamic flow of generalized second grade fluid through porous medium with Hall effects on heat and mass transfer, *Phys. Fluids.*, **32** (2020), 113105. https://doi.org/10.1063/5.0032821
13. Y. H. Jiang, H. G. Sun, Y. Bai, Y. Zhang, MHD flow, radiation heat and mass transfer of fractional Burgers' fluid in porous medium with chemical reaction, *Comput. Math. Appl.*, **115** (2022), 68–79. https://doi.org/10.1016/j.camwa.2022.01.014
14. A. V. Chechkin, R. Gorenflo, I. M. Sokolov, Retarding subdiffusion and accelerating superdiffusion governed by distributed order fractional diffusion equations, *Phys. Rev. E*, **66** (2002), 046129. https://doi.org/10.1103/PhysRevE.66.046129
15. M. Caputo, *Elasticità e dissipazione,* Bologna: Zanichelli, 1969.

16. L. Liu, L. B. Feng, Q. Xu, L. C. Zheng, F. W. Liu, Flow and heat transfer of generalized Maxwell fluid over a moving plate with distributed order time fractional constitutive models, *Int. Commun. Heat Mass Transf.*, **116** (2020), 104679. https://doi.org/10.1016/j.icheatmasstransfer.2020.104679
17. Y. L. Qiao, X. P. Wang, H. Y. Xu, H. T. Qi, Numerical analysis for viscoelastic fluid flow with distributed/variable order time fractional Maxwell constitutive models, *Appl. Math. Mech.-Engl. Ed.*, **42** (2021), 1771–1786. https://doi.org/10.1007/s10483-021-2796-8
18. Z. F. Long, L. Liu, S. Yang, L. B. Feng, L. C. Zheng, Analysis of Marangoni boundary layer flow and heat transfer with novel constitution relationships, *Int. Commun. Heat Mass Transf.*, **127** (2021), 105523. https://doi.org/10.1016/j.icheatmasstransfer.2021.105523
19. W. D. Yang, X. H. Chen, X. R. Zhang, L. C. Zheng, F. W. Liu, Flow and heat transfer of viscoelastic fluid with a novel space distributed-order constitution relationship, *Comput. Math. Appl.*, **94** (2021), 94–103. https://doi.org/10.1016/j.camwa.2021.04.023
20. L. B. Feng, I. Turner, T. Moroney, F. W. Liu, An investigation of space distributed-order models for simulating anomalous transport in a binary medium, *Appl. Math. Comput.*, **434** (2022), 127423. https://doi.org/10.1016/j.amc.2022.127423
21. X. H. Chen, H. B. Xie, W. D. Yang, M. W. Chen, L. C. Zheng, Start-up flow in a pipe of a double distributed-order Maxwell fluid, *Appl. Math. Lett.*, **134** (2022), 108302. https://doi.org/10.1016/j.aml.2022.108302
22. Y. X. Niu, Y. Liu, H. Li, F. W. Liu, Fast high-order compact difference scheme for the nonlinear distributed-order fractional Sobolev model appearing in porous media, *Math Comput Simul*, **203** (2023), 387–407. https://doi.org/10.1016/j.matcom.2022.07.001
23. L. Liu, S. Y. Chen, L. B. Feng, J. Zhu, J. S. Zhang, L. C. Zheng, et al., A novel distributed order time fractional model for heat conduction, anomalous diffusion, and viscoelastic flow problems, *Comput. Fluid.*, **265** (2023), 105991. https://doi.org/10.1016/j.compfluid.2023.105991
24. Y. J. Hu, B. T. Li, C. G. Cao, On viscoelastic blood in a locally narrow artery with magnetic field: application of distributed-order time fractional Maxwell model, *Phys Scr*, **99** (2024), 055018. https://doi.org/10.1088/1402-4896/ad3686
25. M. C. Zhang, F. W. Liu, I. W. Turner, V. V. Anh, Numerical simulation of the distributed-order time-space fractional Bloch-Torrey equation with variable coefficients, *Appl. Math. Model.*, **129** (2024), 169–190. https://doi.org/10.1016/j.apm.2024.01.050
26. W. Ding, S. Patnaik, S. Sidhardh, F. Semperlotti, Applications of distributed-order fractional operators: a review, *Entropy*, **23** (2021), 110. https://doi .org /10.3390 /e23010110
27. L. Liu, L. B. Feng, Q. Xu, Y. P. Chen, Anomalous diffusion in comb model subject to a novel distributed order time fractional Cattaneo–Christov flux, *Appl. Math. Lett.*, **102** (2020), 106116. https://doi.org/10.1016/j.aml.2019.106116
28. I. Podlubny, *Fractional Differential Equations*, San Diego: Academic Press, 1999, 78–85.
29. K. Diethelm, N. J. Ford, Numerical analysis for distributed-order differential equations, *J. Comput. Appl. Math.*, 225 (2009), 96–104. https://doi.org/10.1016/j.cam.2008.07.018
30. K. Diethelm, N. J. Ford, Analysis of Fractional Differential Equations, *J. Math. Anal. Appl.*, **265** (2002), 229–248. https://doi.org/10.1006/jmaa.2000.7194
31. L. Liu, S. Yang, L. B. Feng, Q. Xu, L. C. Zheng, F. W. Liu, Memory dependent anomalous diffusion in comb structure under distributed order time fractional dual-phase-lag model, *Int. J. Biomath.*, **14** (2021), 2150048. https://doi.org/10.1142/S1793524521500480

32. F. Liu, P. Zhuang, V. Anh, I. Turner, K. Burrage, Stability and convergence of the difference methods for the space time fractional advection diffusion equation, *Appl. Math. Comput.*, **191** (2007), 12–20. https://doi.org/10.1016/j.amc.2006.08.162
33. Z. Sun, X. Wu, A fully discrete difference scheme for a diffusion-wave system, *Appl. Numer. Math.*, **56** (2006), 193–209. https://doi.org/10.1016/j.apnum.2005.03.003

AIMS Press